High-performance graphene-integrated thermo-optic switch: design and experimental validation [Invited]

JUNYING LI,[1,9] YIZHONG HUANG,[2,9] YI SONG,[3] LAN LI,[4,5] HANYU ZHENG,[6] HAOZHE WANG,[3] TIAN GU,[6] KATHLEEN RICHARDSON,[7] JING KONG,[3] JUEJUN HU,[6] AND HONGTAO LIN[8,*]

[1]*Shanghai Key Laboratory of Modern Optical Systems, College of Optical-Electrical and Computer Engineering, University of Shanghai for Science and Technology, Shanghai 200093, China*
[2]*Pritzker School of Molecular Engineering, The University of Chicago, Chicago, IL 60637, USA*
[3]*Department of Electrical Engineering & Computer Science, Massachusetts Institute of Technology, Cambridge, MA 02139, USA*
[4]*Key Laboratory of 3D Micro/Nano Fabrication and Characterization of Zhejiang Province, School of Engineering, Westlake University, Hangzhou 310024, China*
[5]*Institute of Advanced Technology, Westlake Institute for Advanced Study, Hangzhou 310024, China*
[6]*Department of Materials Science & Engineering, Massachusetts Institute of Technology, Cambridge, MA 02139, USA*
[7]*The College of Optics & Photonics, University of Central Florida, Orlando, FL 32816, USA*
[8]*College of Information Science & Electronic Engineering, Zhejiang University, Hangzhou 310058, China*
[9]*These authors contributed equally to this work*
hometown@zju.edu.cn

Abstract: The extraordinary optical properties of single-layer graphene have spurred the development of a variety of photonic components. We have previously demonstrated a scalable and versatile platform to facilitate the integration of graphene and other 2-D materials with chalcogenide glass-based planar photonics. In this paper, we detail the design criteria and optimization guidelines towards high-performance graphene-integrated thermo-optic (TO) switches based on the chalcogenide glass-on-graphene platform. Notably, absorption loss of graphene can be reduced to < 20 dB/cm when it is sandwiched inside photonic structures capitalizing on the anisotropic absorption property of graphene. We quantify energy efficiency of the TO switch, showing that the choice of cladding materials plays a critical role in improving device efficiency. Furthermore, we report a record TO switching efficiency of 10 nm/mW via judicious engineering of the overlap between optical mode and thermal profile.

1. Introduction

Optical switches and modulators are essential components for telecommunication and data communications networks [1–3]. Introducing optical switches into a network enables on-demand allocation of bandwidth among different optical links, thereby improving bandwidth resource utilization, reducing power consumption, and mitigating network congestion. Thermo-optic (TO) switching is an appealing approach owing to its potential low power consumption, compact footprint, and ease of integration with integrated photonics platforms. In general, a high-performance TO switch requires smaller footprint, lower insertion loss, high speed, and high energy efficiency (defined as the TO wavelength shift per unit input power in nm/mW), where the latter two are often combinedly characterized by the thermo-optic figure-of-merit (FOM) given as $1/(P_\varphi \cdot \tau)$ (P_φ denotes the product of the TO switching power as defined in [4], and τ denotes the 10%-to-90% rise/fall time). To further scale down the device size and reduce power consumption of the TO switches, a photonic resonator is usually employed to enhance the responsivity of

refractive index with respect to the temperature additionally [5,6]. Currently, TO switches are mainly realized by thermally tuning resonant cavities [7–11] or Mach-Zehnder interferometers (MZIs) [12–15] with metallic [16] or doped silicon micro-heaters [17–23]. State-of-the-art TO switches in general exhibit energy efficiencies between 0.05 to 1 nm/mW and FOMs ranging from 0.01 to 2.6 $mW^{-1} \cdot \mu s^{-1}$ [24–26]. Further enhancing the performance of TO devices is of significant interest for their practical deployment.

Recently, graphene has emerged as a novel efficient heating material in photonic devices [27–29] due to its high electrical conductivity and optical transparency. Graphene-based TO switches with graphene micro-heaters directly attached onto the top of devices in place of traditional metallic heaters has been shown to be an effective method to boost the TO efficiency [30–34]. However, these devices still demand relatively high switching power of the order of milliwatts, which is attributed to poor overlap between the thermal field (which centers on the graphene heater on top of the waveguide) and the optical mode (which primarily resides within the waveguide core). Furthermore, the process of transferring monolayer graphene onto fabricated devices with uneven surface morphology limits process yield, throughput, and scalability. To address the aforementioned limitations, we have recently demonstrated a "monolithic" approach to drastically improve the energy efficiency of graphene TO switch by embedding the 2-D graphene heater in the center of an optical waveguide [4]. Using this approach, we experimentally realized a low switching power consumption of $P_\varphi \sim 110$ μW and a 10%-to-90% rise time of 14 μs, leading to an exceptionally large FOM of 0.65 $mW^{-1} \cdot \mu s^{-1}$.

In this paper, we perform a detailed analysis on the design criteria and optimization guidelines to boost the performance of the waveguide-embedded graphene TO switch decribed in [4]. We start by reviewing the chalcogenide glass-on-graphene integration method and discuss a route to simultaneously achieve low loss and large optical-thermal field overlap in TO switches by sandwiching monolayer graphene at the center of a waveguide. We then investigate the impact of cladding materials on the TO switching energy efficiency. Finally, we optimize the device switching efficiency via engineering a photonic crystal cavity structure to enhance thermal and optical field overlap.

2.   TM-mode transparent graphene-embedded waveguide

Conventionally, graphene integration with photonic components is accomplished by transferring a layer of graphene onto pre-fabricated devices. However, the transfer approach, especially when applied to substrates with uneven patterned surfaces, limits yield, throughput and scalability. Chalcogenide glasses (ChGs), amorphous compounds containing one or more chalcogen elements (S, Se and Te, but excluding O), are broadband transparent infrared materials [35] that uniquely allow room-temperature deposition on various substrates [36–38]. The extremely low thermal budget facilitates its integration with graphene without modifying or disrupting the properties of monolayer graphene. Since wafer-scale graphene transfer onto flat, unpatterned substrate is a well-established process, subsequent chalcogenide film deposition and fabrication enables large-area, high-throughput processing of photonic devices.

Despite its optical transparency to normal incident light, graphene still incurs large optical loss for in-plane propagating modes in waveguides, whether graphene is placed on top of (via transfer) or underneath (via ChG deposition) the waveguide. To illustrate the challenge, we modeled the propagation loss in a strip waveguide made of $Ge_{23}Sb_7S_{70}$ (GSS) chalcogenide glass (with a refractive index of 2.21) at the wavelength of 1550 nm. The loss of a symmetrically cladded waveguide is simulated to be 348 dB/cm for the fundamental transverse electric (TE) mode and 272 dB/cm for the fundamental transverse magnetic (TM) mode when a graphene monolayer is placed underneath the waveguide. As a highly anisotropic optical material, graphene exhibits metallic behavior when interacting with in-plane electric fields and acts as a low-loss dielectric in the out-of-plane direction. Figures 1(a) and (b) show the modal profiles and electric-field

components of the TE and TM modes. Graphene lying under the waveguide (marked by the orange dashed line) interacts with evanescent field of the TE mode and overlaps with the local maxima of in-plane E_z components of TM mode, which results in large optical loss.
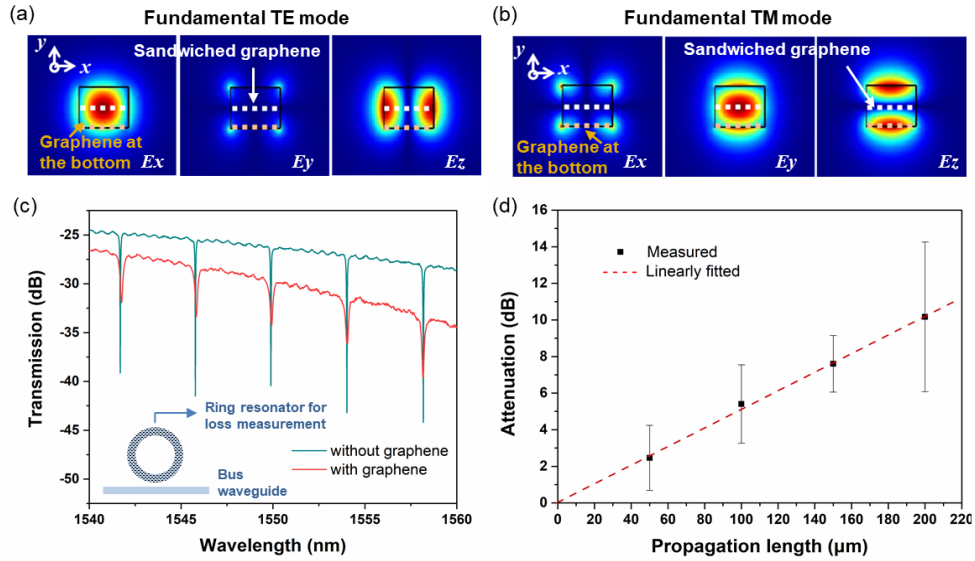

Fig. 1. Graphene sandwiched design with low optical loss: (a, b) profiles of (a) TE-mode and (b) TM-mode electric-field components E_x, E_y and E_z. The orange and white dashed lines in the figure denote the graphene located underneath and embedded inside the waveguide, respectively. (c) Measured TM-mode transmission spectra of a ring resonator with and without a sandwiched graphene layer. (d) Cut-back optical loss quantification of the fundamental TM mode in a GSS waveguide sitting on a graphene layer.

Graphene-sandwiched waveguide structure serves as our validated solution to this dilemma, which achieves a negligible loss for TM mode. As shown in Fig. 1(b), when the graphene is embedded right in the center of the GSS waveguide (marked by the white dash line), it coincides with the node of the in-plane component E_z and only interacts with the E_y out-of-plane component as a dielectric material, leading to a simulated loss of 0 dB/cm for the TM mode. The propagation loss of TM mode was experimentally measured through an all-pass micro-ring resonator (shown in the inset in Fig. 1(c)). The two different transmission spectra in Fig. 1(c) were measured from 40-μm-radius micro-ring resonators with and without embedded graphene. One can see that both the extinction ratio and the loaded Q factor degrade with the incorporation of graphene. From the data, we calculate the propagation loss of the graphene sandwiched waveguide to be (20 ± 2) dB/cm at 1550 nm. An insertion loss of 0.8 dB was measured for a waveguide with 400 μm long graphene [4], consistent with the resonator-based loss quantification. For comparison, the insertion loss of a waveguide with graphene at the bottom was also measured. Figure 1(d) shows attenuation of the fundamental TM mode measured with the cut-back method showing a large loss of (510 ± 7) dB/cm, which is more than 20 times higher than that of the graphene-sandwiched structure.

The results confirm that graphene embedded at the center of photonic waveguides can serve as a TM-transparent heater. Such a sandwiched structure significantly reduces thermal leakage and enhances thermal-optical field overlap since the heating zone is strongly confined inside the waveguide core. This feature is highly advantageous for energy-efficient TO switches.

3.   Impact of waveguide cladding material on TO response

The dielectric cladding outside the waveguide plays an important role in improving the effective TO coefficient of a graphene-integrated TO switch. To elucidate this issue, TO switches based on a graphene-sandwiched Bragg-cavity design were first fabricated with the process flow shown in Fig. 2 and subsequently coated with different cladding materials to evaluate their TO responses. Specifically, a 280-nm thick GSS thin film was thermally evaporated on a 3-μm-oxide-coated silicon wafer followed by wet transfer of monolayer graphene grown via the chemical vapor deposition (CVD) technique [39]. Metal electrodes were defined with the lift-off method, and the graphene layer was then patterned using oxygen plasma etching. Subsequently, another 280-nm thick GSS glass film was deposited before the entire device structure was lithographically defined. Finally, either a layer of PMMA or a drop of index-matching fluid was coated before the measurement.
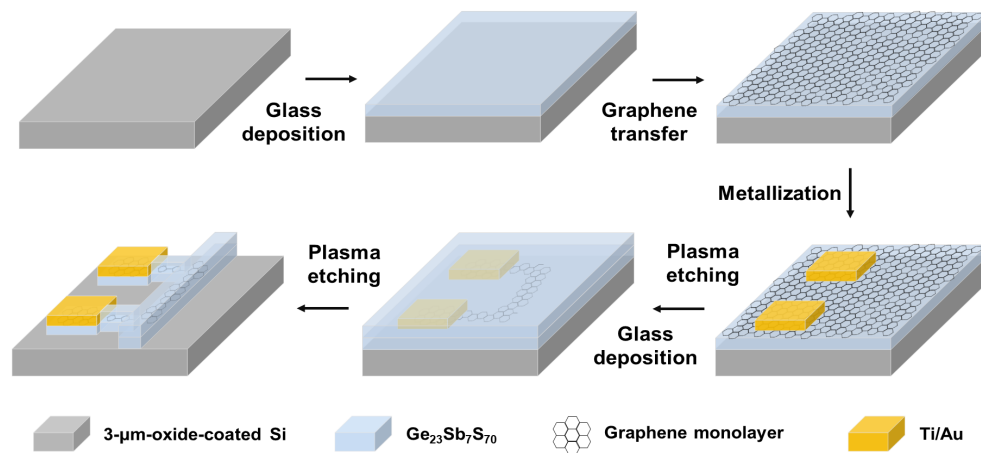

Fig. 2. Schematic fabrication process for the graphene-sandwiched TO switch

Figure 3(a) shows the structure of the graphene-integrated Bragg cavity TO switch. As shown in the yellow dashed line in the middle panel, by using low loss waveguide crossings, the Bragg cavity was connected with metal contact pads through a continuous graphene layer embedded in the middle of the photonic structure. All the switches mentioned in this section share the identical structure parameters (cavity length $L = 10$ μm). The TM-mode transmission spectra of Bragg-cavity based TO switches were measured in different surrounding dielectrics. Figure 3(b) shows the transmission peak drifting versus the varying input power of a TO switch surrounded by an index-matching fluid (IF, refractive index $n_{IF} = 1.46$), while Fig. 3(c) gives the TO response of a device coated with PMMA (refractive index $n_{PMMA} = 1.47$). With increasing input electric power, the resonant peak of the TO switch in the IF case exhibited large blue detuning, whereas only tiny peak shift was observed for the TO switch covered with PMMA. The red and blue dots in Fig. 3(d) mark the measured resonant peak shifts for IF- and PMMA-cladded graphene TO switches and the fittings show clear linear dependency between the peak shift and applied electric power. The fitted energy efficiency of the switch in IF cladding is 0.52 nm/mW, more than 30 times higher than that of the switch in PMMA which is 0.016 nm/mW. This confirms that the dielectric cladding outside the waveguide has a significant impact on the performance of the graphene TO switch.

Light propagating in the waveguide interacts with the surrounding dielectric cladding via the evanescent wave, and the marked performance difference is attributed to the thermo-optic
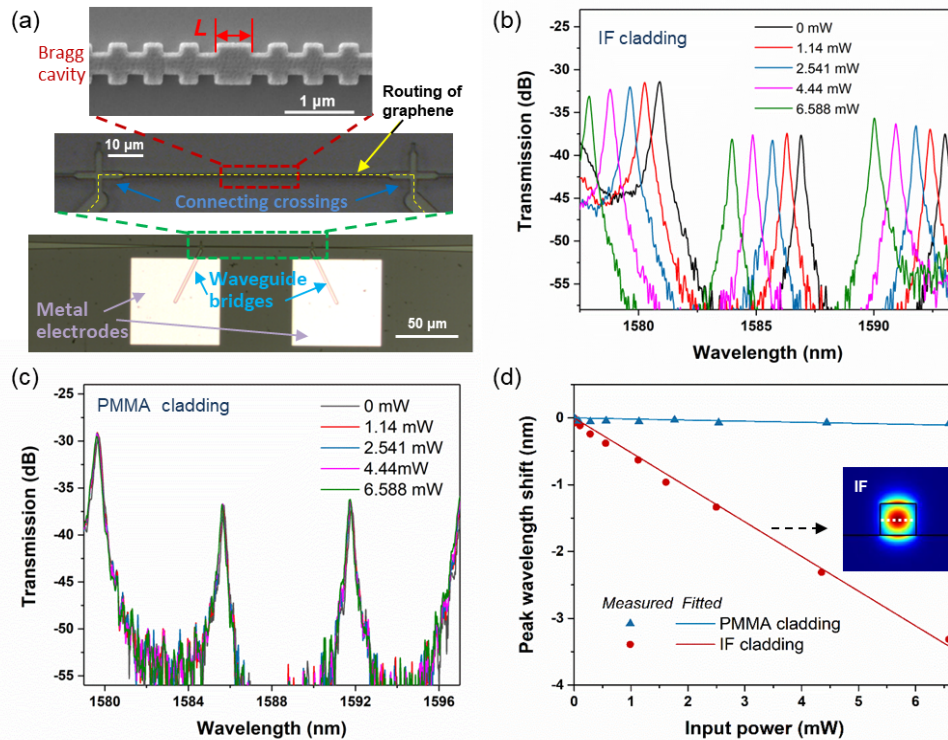
Fig. 3. Graphene-sandwiched Bragg cavity thermo-optic switches with different top claddings. (a) The structure of graphene-sandwiched Bragg cavity TO switch. The waveguide bridges and crossings connecting the electrodes and the Bragg cavity are shown. (b) Transmission spectra of the Bragg cavity switch surrounded by (b) an index-matching fluid and (c) PMMA under varying input electric power. (d) Resonant peak shift of Bragg-cavity-based TO switches with different dielectric claddings (inset: optical modal field intensity in the center of the cavity submerged in IF).

coefficient (TOC) of the cladding materials (see Table 1). In our case, the positive TO response of the GSS chalcogenide waveguide (2.5×10^{-5} K^{-1} [4]) is almost completely cancelled out by PMMA with a negative TOC of -8×10^{-5} K^{-1} [40]. In contrast, IF possesses a large and negative TOC of -6×10^{-4} K^{-1} [4], and thus significantly improves the energy efficiency of the graphene TO switch. Therefore, adopting a cladding material with a high TOC is essential for improving the energy efficiency of TO switch devices.

Table 1. Comparison of energy efficiency of graphene-sandwiched Bragg-cavity thermo-optic switches surrounded by dielectrics with different thermo-optic coefficients.

Cladding material	Thermo-optic coefficient	Energy efficiency of the Bragg cavity based TO switch with different claddings
IF	-6×10^{-4} K^{-1}	0.52 nm/mW
PMMA	-8×10^{-5} K^{-1}	0.016 nm/mW

Since the cladding is the main TO medium in our design, enhancing evanescent field is supposed to further improve the TO response of the switch. In the design shown in Fig. 3(a), most of the optical field is confined inside the GSS waveguide, as the modal field intensity shows

in the inset of Fig. 3(d). In the next section, we discuss alternative cavity designs exhibiting stronger evanescent field to further improve the device performance.

4.   Optimizing photonic crystal cavity design

To meet the aforementioned requirements, we designed a TO switch with strongly transverse modal delocalization. As illustrated schematically in Fig. 4(a), the cavity consists of a 600 nm wide rectangular block array (labelled as mirror units) with a period of 480 nm and a duty cycle of 0.5 to operate near 1.57 μm wavelength. The cavity has a uniform waveguide height of 560 nm to support the TM mode. In contrast to the Bragg cavity shown in Fig. 3, this 1-D nanobeam photonic crystal resonator assumes a zero-length cavity design to minimize the mode volume [41]. The block-to-block spacing is kept constant while the width of the waveguide connecting the blocks is quadratically tapered down from W_{PhC_b} (the initial waveguide width) to W_{PhC_min} (the minimum waveguide width at the center of the photonic crystal cavity) to create a Gaussian-like potential well in the photonic bandgap. The waveguide width tapering profile follows the equation:

$$W_{PhC}(ii) = W_{PhC\_b} + \frac{W_{PhC\_b} - W_{PhC\_\min}}{N^2} ii^2 \tag{1}$$

where N denotes the number of the block unit on each side of the photonic crystal cavity, and $W_{PhC}(ii)$ denotes the width of iith block-connecting waveguide in the cavity ($ii \leq N$). With this design, the cavity seamlessly couples to the input/output waveguides without additional coupling waveguide sections since the waveguide width W_{PhC} approaches that of the feeding waveguide at both ends of the Bragg cavity.

   In our dielectric-mode photonic crystal cavity (PhC), the cavity intrinsic Q factor (Q_{in}) and external Q factor (Q_{ex}) are determined by the radiative loss from the cavity to free space and the coupling loss between the cavity and the input/output waveguides. In general, Q_{ex} can be improved by simply increasing the number of block units N as the mirror strength linearly increases as a function of N. As shown in Fig. 4(b), higher loaded Q was obtained with larger N, and meanwhile the transmission of the cavity decreased due to the fact that the PhC operates in the under coupling regime ($Q_{ex} > Q_{in}$). While cavity Q does not directly affect the energy efficiency, higher Q is beneficial for reducing the switching energy since less peak detuning is needed to produce the desired intensity modulation. Taking into account the tradeoff between the Q factor and cavity transmission, we set the unit number N to 45 (Fig. 4(d)).

   We also emphasize here that another critical parameter for improving the performance of the TO switch is the waveguide width (W_{PhC}), or rather, the minimum waveguide width (W_{PhC_min}) at the center of cavity. Smaller W_{PhC_min} is preferred because:

   1) it leads to a higher Q factor by increasing the mirror strength (see Fig. 4(d));

   2) it yields stronger evanescent field into the cladding (see insert of Fig. 4(d)); and

   3) it defines a narrower graphene channel with higher electrical resistance [33]. According to the voltage divider rule, the electric power allocated at these narrow areas is higher compared to at the locations with wider graphene (i.e. at the blocks). Consequently, heat generation is larger at the center of the cavity than near the feeder waveguides. This can be seen from Fig. 4(c), which plots the electrical resistances and the thermal power generation of each unit (i.e. a block plus a narrow waveguide segment connecting two neighboring blocks) in the cavity. It is evident that the heat generation profile has a maximum coinciding with the center of the photonic cavity where the optical mode is most concentrated. For all the reasons above, we conclude that small W_{PhC_min} significantly boosts the device energy efficiency.
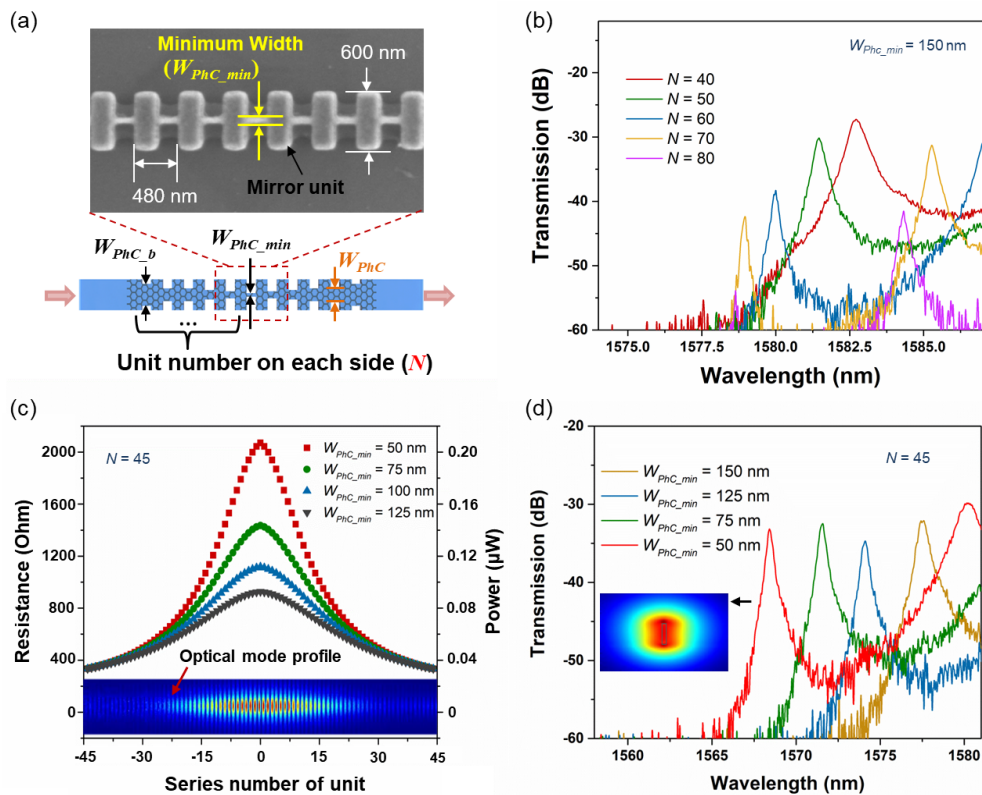
Fig. 4. (a) Schematic diagram of a graphene-sandwiched zero-length photonic crystal cavity TO switch, and an SEM image of the local structure at the center of the cavity. The graphene layer is connected with electrodes in the same manner as the Bragg cavity TO switch. (b) Transmission spectra of photonic crystal cavities with varying number of units N (W_{PhC_min} = 150 nm). (c) Electrical resistances of each mirror unit and the corresponding thermal power generated at each unit (with 10 μA current input) in the graphene-sandwiched cavity with $N = 45$ and different W_{PhC_min}. The cavity mode profile was also shown at the bottom panel to illustrate the thermal-optical field overlap. The sheet resistance of graphene was taken as 400 ohm/sq following our experimental measurement results. (d) Transmission spectra of the photonic crystal cavity with different W_{PhC_min} ($N = 45$).

Along this line, we investigated the TO switching performance based on the geometrically optimized design of $N = 45$ and $W_{PhC\_min} = 50$ nm. The transmission spectra at different input electrical power levels shown in Fig. 5(a) allow us to fit an energy efficiency of the optimized device to be 7.6 nm/mW. The lowest measured insertion loss of our TO switches is approximately 2 dB. The insertion loss mainly comes from fabrication imperfections (including scattering loss from sidewall roughness and absorption from uneven graphene during transfer). Through further fabrication processes optimization, the insertion loss can be minimized. The TO switch device reported in [4] follows the same design parameters although with improved graphene transfer and handling processes to further reduce the contact resistance, yielding a record 10 nm/mW TO energy efficiency. As shown in Fig. 5(b), this design indeed exhibits higher efficiency than other switch designs with larger W_{PhC_min}. Note that the performance of all of the photonic crystal TO switches is consistently higher than even the best performance achieved in the simple Bragg cavity TO switch (Fig. 3), which validates the aforementioned advantages of the zero-length photonic crystal cavity design.
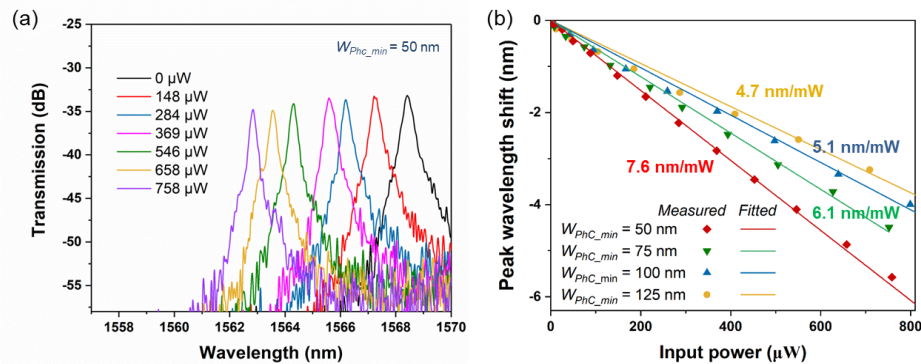

Fig. 5. (a) As-measured transmission spectra of an optimized graphene-sandwiched photonic crystal TO switch ($W_{PhC\_min} = 50$ nm, $N = 45$) with varying input power levels. (b) Measured peak wavelength shift (dots) and fitted energy efficiency (lines) of the photonic crystal TO switches with varying minimum waveguide width W_{PhC_min} ($N = 45$).

The switching energy P_φ of the optimized TO switch is 0.11 mW, which is on par with the record-low power consumption achieved in TO switch with suspended structures [42]. Among TO switches with the same level of power consumption, our device claims the fastest response (10%-to-90% rise time of 14 μs). Hence, following the design route described above, graphene-integrated TO switches with record-high energy efficiency, small device footprint and low power consumption can be realized.

5. Conclusion

In conclusion, design guidelines and optimization strategies have been proposed and experimentally verified with the aim of reducing the power consumption and improving the energy efficiency of graphene-integrated TO switches. By harnessing the anisotropic absorption property of graphene, we show that the insertion loss of the graphene integrated devices can be fully nullified for the TM mode with a graphene-sandwiched structure. In addition, such a design also benefits from excellent confinement of the thermal field in the waveguide with maximum overlap with the optical mode. We found that by altering the cladding material over the cavity, it is possible to modify the effective TOC of the entire cavity, thereby enhancing its TO performance. Besides, we demonstrate that the heating efficiency can be further improved with an optimized deign of

the photonic crystal cavity to achieve optimal overlap between the optical mode and thermal generation profile. The switch performance can be further improved by leveraging additional enhancement effects (including slow-light effect [26,34] and slot effect [43]). We believe that these design rules can be easily transferred to optimizing other photonic devices such as 2-D material integrated modulators and filters, and potentially pave the way towards wafer-scale, high-performance photonics based on 2-D materials.

Funding

Acknowledgements

References

1. Q. Cheng, M. Bahadori, M. Glick, S. Rumley, and K. Bergman, "Recent advances in optical technologies for data centers: a review," Optica **5**(11), 1354–1370 (2018).
2. Q. Cheng, S. Rumley, M. Bahadori, and K. Bergman, "Photonic switching in high performance datacenters," Opt. Express **26**(12), 16022–16043 (2018).
3. N. Farrington, G. Porter, S. Radhakrishnan, H. H. Bazzaz, V. Subramanya, Y. Fainman, G. Papen, and A. Vahdat, "Helios: a hybrid electrical/optical switch architecture for modular data centers," SIGCOMM Comput. Commun. Rev. **40**(4), 339–350 (2010).
4. H. Lin, Y. Song, Y. Huang, D. Kita, S. Deckoff-Jones, K. Wang, L. Li, J. Li, H. Zheng, Z. Luo, H. Wang, S. Novak, A. Yadav, C. C. Huang, R. J. Shiue, D. Englund, T. Gu, D. Hewak, K. Richardson, J. Kong, and J. Hu, "Chalcogenide glass-on-graphene photonics," Nat. Photonics **11**(12), 798–805 (2017).
5. C. A. Barrios, V. R. de Almeida, and M. Lipson, "Low-power-consumption short-length and high-modulation-depth silicon electrooptic modulator," J. Lightwave Technol. **21**(4), 1089–1098 (2003).
6. V. R. Almeida, C. A. Barrios, R. R. Panepucci, and M. Lipson, "All-optical control of light on a silicon chip," Nature **431**(7012), 1081–1084 (2004).
7. M. S. Nawrocka, T. Liu, X. Wang, and R. R. Panepucci, "Tunable silicon microring resonator with wide free spectral range," Appl. Phys. Lett. **89**(7), 071110 (2006).
8. M. W. Pruessner, T. H. Stievater, M. S. Ferraro, and W. S. Rabinovich, "Thermo-optic tuning and switching in SOI waveguide Fabry-Perot microcavities," Opt. Express **15**(12), 7557–7563 (2007).
9. J. Gosciniak, S. I. Bozhevolnyi, T. B. Andersen, V. S. Volkov, J. K. Hansen, L. Markey, and A. Dereux, "Thermo-optic control of dielectric-loaded plasmonic waveguide components," Opt. Express **18**(2), 1207–1216 (2010).
10. C. Tapalian, J. P. Laine, and P. A. Lane, "Thermo-optical switches using coated microsphere resonators," MRS Online Proceedings Library Archive, 694 (2001).
11. D. Armani, B. Min, A. Martin, and K. J. Vahala, "Electrical thermo-optic tuning of ultrahigh-Q microtoroid resonators," Appl. Phys. Lett. **85**(22), 5439–5441 (2004).
12. S. Chen, Y. Shi, S. He, and D. Dai, "Low-loss and broadband 2× 2 silicon thermo-optic Mach–Zehnder switch with bent directional couplers," Opt. Lett. **41**(4), 836–839 (2016).
13. M. R. Watts, J. Sun, C. DeRose, D. C. Trotter, R. W. Young, and G. N. Nielson, "Adiabatic thermo-optic Mach–Zehnder switch," Opt. Lett. **38**(5), 733–735 (2013).
14. K. Liu, C. Zhang, S. Mu, S. Wang, and V. J. Sorger, "Two-dimensional design and analysis of trench-coupler based Silicon Mach-Zehnder thermo-optic switch," Opt. Express **24**(14), 15845–15853 (2016).
15. M. W. Geis, S. J. Spector, R. C. Williamson, and T. M. Lyszczarz, "Submicrosecond submilliwatt silicon-on-insulator thermooptic switch," IEEE Photonics Technol. Lett. **16**(11), 2514–2516 (2004).
16. B. S. Lee, M. Zhang, F. A. S. Barbosa, S. A. Miller, A. Mohanty, R. St-Gelais, and M. Lipson, "On-chip thermo-optic tuning of suspended microresonators," Opt. Express **25**(11), 12109–12120 (2017).
17. P. Dong, W. Qian, H. Liang, R. Shafiiha, D. Feng, G. Li, J. E. Cunningham, A. V. Krishnamoorthy, and M. Asghari, "Thermally tunable silicon racetrack resonators with ultralow tuning power," Opt. Express **18**(19), 20298–20304 (2010).

18. D. Englund, B. Ellis, E. Edwards, T. Sarmiento, J. S. Harris, D. A. B. Miller, and J. Vučković, "Electrically controlled modulation in a photonic crystal nanocavity," Opt. Express **17**(18), 15409–15419 (2009).

19. M. Zhang, G. S. Wiederhecker, S. Manipatruni, A. Barnard, P. McEuen, and M. Lipson, "Synchronization of micromechanical oscillators using light," Phys. Rev. Lett. **109**(23), 233906 (2012).

20. M. R. Watts, "Adiabatic microring resonators," Opt. Lett. **35**(19), 3231–3233 (2010).

21. D. Kita, B. Miranda, D. Favela, D. Bono, J. Michon, H. Lin, T. Gu, and J. Hu, "High-performance and scalable on-chip digital Fourier transform spectroscopy," Nat. Commun. **9**(1), 4405 (2018).

22. Y. Shen, N. C. Harris, S. Skirlo, M. Prabhu, T. B. Jones, M. Hochberg, X. Sun, S. Zhao, H. Larochelle, D. Englund, and M. Soljačić, "Deep learning with coherent nanophotonic circuits," Nat. Photonics **11**(7), 441–446 (2017).

23. N. C. Harris, G. R. Steinbrecher, M. Prabhu, Y. Lahini, J. Mower, D. Bunandar, C. Chen, F. N. C. Wong, T. Baehr-Jones, M. Hochberg, S. Lloyd, and D. Englund, "Quantum transport simulations in a programmable nanophotonic processor," Nat. Photonics **11**(7), 447–452 (2017).

24. X. Li, H. Xu, X. Xiao, Z. Li, Y. Yu, and J. Yu, "Fast and efficient silicon thermo-optic switching based on reverse breakdown of pn junction," Opt. Lett. **39**(4), 751–753 (2014).

25. J. V. Campenhout, W. M. J. Green, S. Assefa, and Y. A. Vlasov, "Integrated NiSi waveguide heaters for CMOS-compatible silicon thermo-optic devices," Opt. Lett. **35**(7), 1013–1015 (2010).

26. Y. A. Vlasov, M. O'boyle, H. F. Hamann, and S. J. McNab, "Active control of slow light on a chip with photonic crystal waveguides," Nature **438**(7064), 65–69 (2005).

27. J. Kang, H. Kim, K. S. Kim, S. K. Lee, S. Bae, J. H. Ahn, Y. J. Kim J, B. Choi, and B. H. Hong, "High-performance graphene-based transparent flexible heaters," Nano Lett. **11**(12), 5154–5158 (2011).

28. D. Sui, Y. Huang, L. Huang, J. Liang, Y. Ma, and Y. Chen, "Flexible and transparent electrothermal film heaters based on graphene materials," Small **7**(22), 3186–3192 (2011).

29. Z. Sun, A. Martinez, and F. Wang, "Optical modulators with 2D layered materials," Nat. Photonics **10**(4), 227–238 (2016).

30. S. Gan, C. Cheng, Y. Zhan, B. Huang, X. Gan, S. Li, S. Lin, X. Li, J. Zhao, H. Chen, and Q. Bao, "A highly efficient thermo-optic microring modulator assisted by graphene," Nanoscale **7**(47), 20249–20255 (2015).

31. L. Yu, D. Dai, and S. He, "Graphene-based transparent flexible heat conductor for thermally tuning nanophotonic integrated devices," Appl. Phys. Lett. **105**(25), 251104 (2014).

32. C. Qiu, Y. Yang, C. Li, Y. Wang, K. Wu, and J. Chen, "All-optical control of light on a graphene-on-silicon nitride chip using thermo-optic effect," Sci. Rep. **7**(1), 17046 (2017).

33. L. Yu, Y. Yin, Y. Shi, D. Dai, and S. He, "Thermally tunable silicon photonic microdisk resonator with transparent graphene nanoheaters," Optica **3**(2), 159–166 (2016).

34. S. Yan, X. Zhu, L. H. Frandsen, S. Xiao, N. A. Mortensen, J. Dong, and Y. Ding, "Slow-light-enhanced energy efficiency for graphene microheaters on silicon photonic crystal waveguides," Nat. Commun. **8**(1), 14411 (2017).

35. Q. Du, Y. Huang, J. Li, D. Kita, J. Michon, H. Lin, L. Li, S. Novak, K. Richardson, W. Zhang, and J. Hu, "Low-loss photonic device in Ge-Sb-S chalcogenide glass," Opt. Lett. **41**(13), 3090 (2016).

36. L. Li, H. Lin, S. Qiao, Y. Huang, J. Li, J. Michon, T. Gu, C. Alosno-Ramos, L. Vivien, A. Yadav, K. Richardson, N. Lu, and J. Hu, "Monolithically Integrated Stretchable Photonics," Light: Sci. Appl. **7**(2), 17138 (2018).

37. L. Li, H. Lin, Y. Huang, R. Shiue, A. Yadav, J. Li, J. Michon, D. Englund, K. Richardson, T. Gu, and J. Hu, "High-performance flexible waveguide-integrated photodetectors," Optica **5**(1), 44–51 (2018).

38. J. Hu, L. Li, H. Lin, Y. Zou, Q. Du, C. Smith, S. Novak, K. Richardson, and J. D. Musgraves, "Chalcogenide glass microphotonics: Stepping into the spotlight," Am. Ceram. Soc. Bull. **94**(4), 24–29 (2015).

39. J. Y. Hong, Y. C. Shin, A. Zubair, Y. Mao, T. Palacios, M. S. Dresselhaus, S. H. Kim, and J. Kong, "A rational strategy for graphene transfer on substrates with rough features," Adv. Mater. **28**(12), 2382–2392 (2016).

40. D. I. Johnson and G. E. Town, "Refractive index and thermo-optic coefficient of composite polymers at 1.55 μm," Proc. SPIE **6038**, 603821 (2005).

41. Q. Quan, P. B. Deotare, and M. Loncar, "Photonic crystal nanobeam cavity strongly coupled to the feeding waveguide," Appl. Phys. Lett. **96**(20), 203102 (2010).

42. Z. Lu, K. Murray, H. Jayatilleka, and L. Chrostowski, "Michelson interferometer thermo-optic switch on SOI with a 50 microwatt power consumption," IEEE Photonics Technol. Lett. **27**(22), 2319–2322 (2015).

43. M. S. Kwon, "Discussion of the epsilon-near-zero effect of graphene in a horizontal slot waveguide," IEEE Photonics J. **6**(3), 1–9 (2014).